PRELIMINARY MEASUREMENTS WITH A COMPTON-SUPPRESSED PHOSWICH DETECTOR

Abi T. Farsoni, Bemnet Alemayehu, and Abdulsalam M. Alhawsawi

Oregon State University

Sponsored by the National Nuclear Security Administration

Award No. DE-AC52-09NA29324
Proposal No. BAA09-27

ABSTRACT

Monitoring atmospheric radioxenon is a key component of the International Monitoring System to verify any underground nuclear weapon tests around the world. Several detectors have been designed and tested for radioxenon measurements during the last two decades. Most of these detectors employ the beta-gamma coincidence technique to measure xenon radioisotopes. This technique can significantly reduce the spectral background in the X-ray/gamma-ray spectrum and increase the overall system sensitivity. One important parameter in evaluating the sensitivity of these systems for radioxenon measurement is the Minimum Detectable Concentration (MDC) for each radioxenon in the atmosphere. The MDC for a particular radioisotope can be improved by reducing the spectral background at the region of interest of gamma-ray spectrum. Detectors designed based on beta-gamma coincidence measurements show a significant reduction in spectral background from external sources. However, they are still suffering a background component in the two-dimensional beta-gamma coincidence spectrum due to Compton scattering events originated from high-energy gamma sources in the sample gas (e.g., Radon daughters).

A phoswich detector with Compton suppression capability has been developed and assembled for measuring low concentration of xenon radioisotopes in the atmosphere. The phoswich detector has been designed with three scintillation layers. Beta-gamma coincidence events from radioxenon isotopes are identified when a coincidence energy absorption is detected from the first (plastic, BC-400) and second (CsI(Tl) crystal) scintillation layers. To identify and reject scattered photons from CsI(Tl) crystal, this crystal is surrounded by a bismuth germinate (BGO) scintillation layer. The Compton suppression capability of the detector effectively reduces the Compton continuum in the two-dimensional gamma-beta coincidence spectra and can significantly improve the Minimum Detectable Concentration (MDC) of the xenon radioisotopes. In this paper, detector assembly steps and our preliminary measurements with lab sources and radioxenon isotopes produced in the Oregon State University TRIGA reactor will be discussed.

OBJECTIVE

The International Monitoring System (IMS) installed and employs radioxenon detectors in various locations to verify nuclear weapons test around the world. Several detectors have been designed and tested for radioxenon measurements during the last two decades. Most of these detectors employ the beta-gamma coincidence technique to measure xenon radioisotopes. This technique can significantly reduce the spectral background in the X-ray/gamma-ray spectrum and increase the overall system sensitivity. One important parameter in evaluating the sensitivity of these systems for radioxenon measurement is the MDC for each radioxenon in the atmosphere. The MDC for a particular radioisotope can be improved by reducing the spectral background at the region of interest of gamma-ray spectrum. Detectors designed based on beta-gamma coincidence measurements show a significant reduction in spectral background from external sources. However, they are still suffering a background component in the two-dimensional beta-gamma coincidence spectrum due to Compton scattering events originated from high-energy gamma sources in the sample gas (e.g. Radon daughters).

Phoswich detectors have recently been considered as an alternative to simplify radioxenon detection (Ely et al., 2003; Hennig et al., 2005; Farsoni et al., 2008). In a phoswich detector, two or more scintillation layers are coupled to a single photomultiplier tube (PMT). The energy deposition in each layer from incident beta and/or gamma, in coincidence or singles, is then determined via digital pulse shape analysis of the PMT's anode pulses.

A phoswich detector has been designed and constructed to measure xenon radioisotopes via beta-gamma coincidence technique. One important feature of this detector in enhancing the radioxenon detection is its capability to identify and reject Compton scattering events in its gamma energy spectrum. The Compton suppression mechanism is integrated into the phoswich design to effectively reduce the Compton continuum in 2D gamma-beta coincidence spectra and significantly improve the MDC of the xenon radioisotopes. In this paper, after describing the detector design and assembly, we will present our recent measurements with radioactive lab sources and xenon radioisotopes produced in the TRIGA reactor at the Oregon State University.

RESEARCH ACCOMPLISHED

Design and Assembly of the Phoswich Detector

A phoswich detector with Compton suppression capability has been designed and constructed to measure xenon radioisotopes via beta-gamma coincidence technique. As depicted in Figure 1, the phoswich detector has been designed with three scintillation layers: a thin plastic scintillator to detect beta and conversion electrons, a CsI(Tl) crystal for measuring X-rays and gamma-rays and a BGO crystal, which surrounds the CsI(Tl) layer, to identify scattered photons and ultimately reducing Compton continuum in the gamma energy spectrum. In this paper, we will call this detector: "Actively-Shielded Phoswich" (ASP) detector.

The BGO crystal is a high-dense (7.13 g/cm^3) and high-efficient scintillator and is commonly used in Compton suppression systems. This scintillator is integrated into our phoswich detector to identify and reject unwanted Compton scatters in the CsI(Tl) crystal from internal and external gamma-ray sources. Besides, the decay time of BGO crystal (300 nsec) is well different from the other two scintillators (2.4 nsec of BC-400 and ~1,000 nsec of CsI[Tl]). This will facilitate our digital pulse shape analysis algorithm in discriminating the origin of radiation interactions.

Previous tests on the Automated Radioxenon Sampler and Analyzer (ARSA, McIntyre et al., 2001) have shown that latent radioxenon remains in the gas cells even after evacuation of the gases, leading to a memory effect which increases the background level for subsequent measurements. Therefore, to minimize this effect, a very thin layer of aluminum (1 μm) was deposited on the surface of the plastic scintillator (BC-400). The aluminum coating process was performed using a vacuum coating process at the Oregon State University.

To have full flexibility in customizing the phoswich detector, we assembled the detector in our lab. The BC-400 and the BGO crystal are not hygroscopic but the CsI(Tl) crystal is slightly hygroscopic. Therefore, to minimize dead layer buildup on the surface of CsI(Tl), the crystal should not be exposed to a humidity more than 20% during the assembly. This was recommended by the crystal supplier (Saint-Gobain Crystals). To obtain this condition, all assembly materials including CsI(Tl) were placed inside a plastic glove bag. To reduce the humidity inside the glove bag, three trays of Indicating Drierite desiccant (as moisture absorber) were placed in the bag. Then the bag was sealed and filled with nitrogen gas. After 14 days, when the humidity inside the bag reached below 15%, the detector assembly was started.

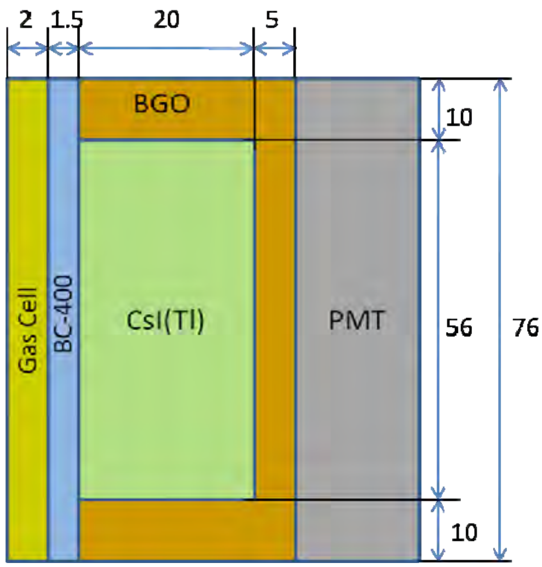

Figure 1. Schematic diagram of Actively-Shielded Phoswich (ASP) detector. All dimensions are in mm.

To have an optical coupling between BGO and CsI(Tl), a layer of silicone grease (BC-630, Saint-Gobain Crystals) was smeared inside the BGO crystal. CsI(Tl) was then placed inside the BGO crystal. The CsI(Tl) crystal was rotated inside the BGO in different directions to remove any remaining air bubbles, and to uniformly distribute the silicone grease between the crystals. The gaps between BC-400 and BGO-CsI(Tl) and between BGO and PMT (R1307-07, Hamamatsu) glass window were filled with a thin layer of silicone grease as well. The PMT and scintillators were wrapped with 5 layers of Teflon. The assembly was then wrapped with plastic wrap to maintain the integrity of the assembly. Then, the whole scintillation assembly was placed and fastened inside aluminum housing as shown in Figure 2.

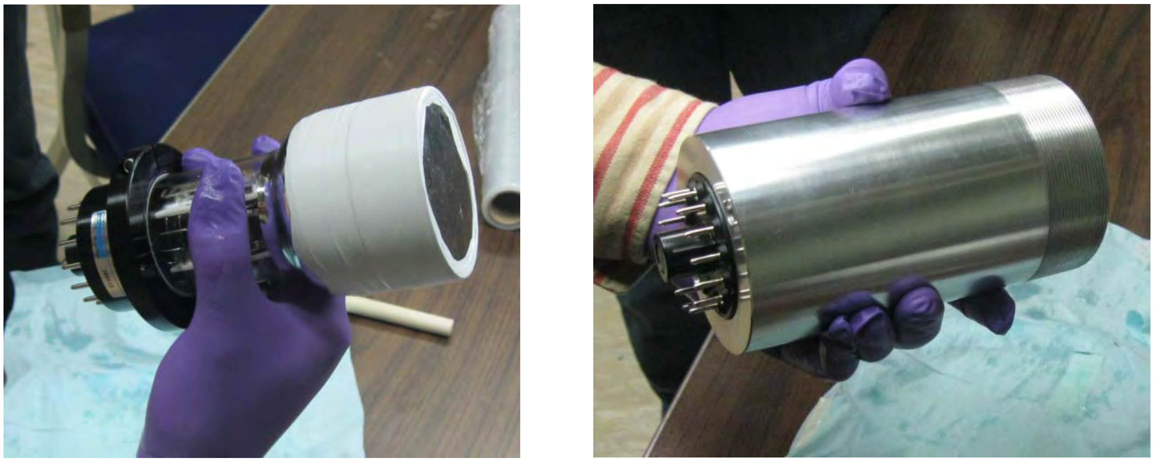

Figure 2. The whole scintillation assembly and PMT (R1307-07, Hamamatsu) were placed inside the detector aluminum housing.

Digital Pulse Shape Discrimination

In this work, we used a 200 MHz digital spectrometer (RX1200) from Avicenna Instruments LLC to digitally process anode pulses from the ASP detector. The RX1200 is a user-programmable digital spectrometer. The on-board Field-Programmable Gate Array (FPGA) in RX1200 can be programmed via USB2 port. For development purposes, we used an offline analysis using the MATLAB software to digitally process pulses from our phoswich detector.

Coincidence (and Compton-suppressed) events are discriminated from single events using digital pulse shape analysis. Two parameters (Fast and Slow Component Ratios, FCR and SCR) are calculated from each incoming pulse to discriminate different pulse shapes or events (Farsoni at al., 2008). The FCR and SCR range from zero to unity. Figure 3 shows a two-dimensional scatter plot of the FCR and SCR when the ASP detector was exposed to a ^{137}Cs source. During this experiment, the ^{137}Cs source was shielded against beta and conversion electrons. Depending on how the incident gamma-ray releases its energy within each layer of the phoswich detector, seven possible regions will be populated in the FCR-SCR scatter plot. Regions 1, 2 and 4 represent single events in plastic (BC-400), CsI(Tl) and BGO scintillators, respectively. Regions 3 and 5 show coincidence events of CsI(Tl)-plastic and BGO-plastic, respectively. Region 6 accommodates Compton scattering events between CsI(Tl) and BGO. When either all three timing components appear in the pulse or the shape of pulse is unknown, the corresponding event appears in region 7.

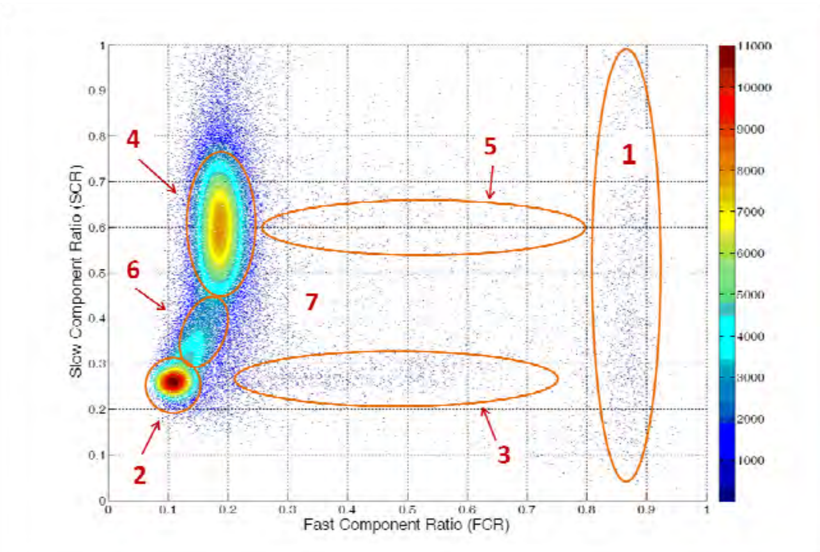

Figure 3. Scatter of Fast and Slow Component Ratios from ^{137}Cs. Seven marked regions correspond to seven pulse shapes, indicating how gamma-rays interact with the three layers of phoswich detector.

Compton Suppression

While region 2 in Figure 3 is populated from single events in CsI(Tl), coincidence energy depositions in CsI(Tl) and BGO will record events in region 6. Therefore, events in region 2 were used to collect a gamma spectrum with minimum Compton scattering in CsI(Tl) crystal (suppressed spectrum). To collect an unsuppressed gamma spectrum, events in both regions (2 and 6) were used because in case of a Compton scattering in CsI(Tl) and a consequent energy absorption in BGO, the corresponding event moves from region 2 to region 6.

The primary FPGA design was modified to characterize the phoswich detector in suppressing the Compton events in the gamma spectrum. The suppressed and unsuppressed spectra, presented in Figure 4, were collected using complete real-time digital pulse processing in the FPGA when the phoswich detector was exposed to 662 keV gamma-rays from ^{137}Cs. To collect these spectra, a 4096 x 32-bit energy histogram was implemented from eight Block RAMs in the FPGA. The histogram was updated only if the measured FCR-SCR values of the pulses fell into a predetermined FCR-SCR region (region 2 alone or regions 2 and 6 in Figure 3 for suppressed or unsuppressed spectra, respectively). In these experiments, to minimize BGO contribution in measuring the corresponding energy absorption in CsI(Tl) crystal, only tailing portions of each pulse were integrated (500 nanoseconds to 5,000 nanoseconds after the trigger). This approximation degrades the CsI(Tl) energy resolution due to an incomplete pulse integration process. However, a small contribution from the BGO crystal was observed in the low-energy portion of both suppressed and unsuppressed gamma spectra shown in Figure 4. The energy resolution of the 662 keV peak in both spectra in Figure 4 was measured to be 10.2%.

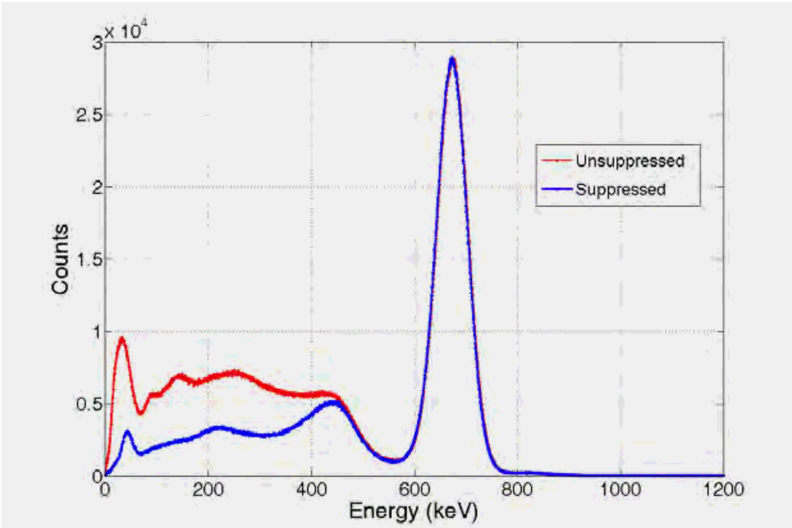

Figure 4. Suppressed and unsuppressed gamma-ray spectra from ^{137}Cs.

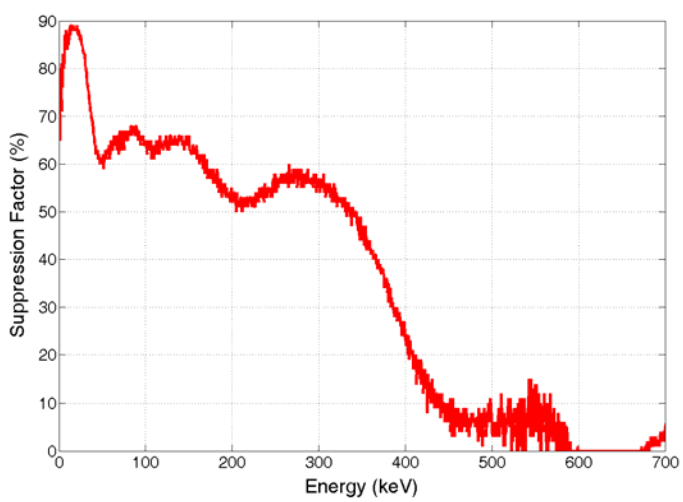

Figure 5. Suppression factors as a function of photon energy.

To study the Compton suppression mechanism of the phoswich detector for energy spectra presented in Figure 4, the suppression factor was defined as:

$$\text{Suppression Factor (E)} = \frac{C_u(E) - C_s(E)}{C_u(E)} \times 100$$

where: $C_u(E)$ is the number of counts in energy E of the unsuppressed spectrum

$C_s(E)$ is the number of counts in energy E of the suppressed spectrum

Figure 5 shows the resulting suppression factor as a function of photon energy. In this figure, events below about 50 keV should be ignored since the low-energy peak that appeared in the unsuppressed spectrum is believed to be from the BGO contribution. Figure 5 shows that the Compton suppression mechanism is more efficient (50%-60%) in the low-energy part of the Compton continuum than the higher energies close to the Compton edge (~477 keV). This complies with this fact that because CsI(Tl) crystal is not surrounded by the BGO crystal at the front window, the BGO cannot detect high-angle scattered photons and as a result the Compton mechanism should be more efficient in rejecting low-angle scattered photons from CsI(Tl) scintillator. Events very close to the Compton edge correspond to about 180-degree scattered events and will likely escape the detector without releasing any energy in the BGO.

Another useful parameter which is generally used to characterize the Compton suppression capability is the peak-to-Compton ratio. The peak-to-Compton ratio for the ^{137}Cs 662 keV gamma ray is defined to be the ratio of highest counts in the photopeak to the average counts from 358-382 keV in the Compton continuum (ANSI/IEEE Standards 325, 1986). The peak-to-Compton ratios for the unsuppressed and suppressed spectra shown in Figure 4 were calculated to be 5.1 and 8.2, respectively.

Radioxenon Measurements

To find the optimum settings for our pulse shape discrimination analysis and to characterize the detector in measuring xenon radioisotopes (^{135}Xe and ^{133}Xe), small volumes (3 ml) of stable and enriched (>99%) isotopes of xenon, ^{134}Xe and ^{132}Xe, were irradiated in the thermal column of the TRIGA reactor for two hours. The thermal neutron flux for this irradiation was $7\text{x}10^{10}$ n/cm^{-2}/sec^{-1}. Details about the gas transfer manifold and procedures are explained elsewhere (Farsoni et al., 2010).

^{135}Xe measurements

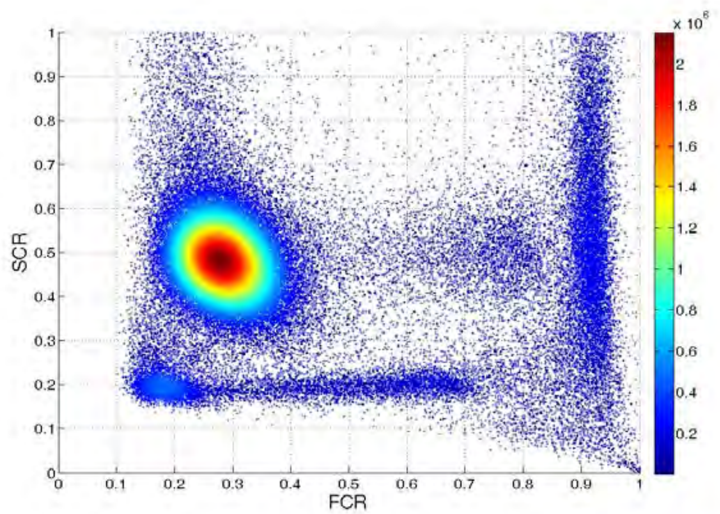

Figure 6. Scatter of Fast and Slow Component Ratios from ^{135}Xe.

Figure 6 presents the FCR-SCR scatter plot when the ASP detector was exposed to ^{135}Xe. All major pulse-shape regions including beta-gamma coincidence region (region 3, when both BC-400 and CsI(Tl) detect coincidence energy absorption) can be identified in this figure. As it can be seen in this figure, region 4 (BGO's single events) is much more populated than region 2 (CsI's single events). This did not comply with our previous radiation transport modeling. After this experiment and by examining the detector, we noticed that the radioxenon gas had been leaked from the gas cell into the space between scintillation assembly and aluminum housing during the measurement. This exposed the external surface of BGO crystal directly to both beta and gamma radiation and resulted in a direct energy absorption in this layer. This problem was fixed for the rest of these experiments by filling the gap using a general purpose insulating foam sealant.

The resulting two-dimensional beta-gamma coincidence energy spectrum from ^{135}Xe is shown in Figure 7. Horizontal and vertical axes in this figure represent energy deposition in BC-400 and CsI(Tl), respectively. Gamma-ray energy spectra from region 2 (suppressed, single events) and region 3 (suppressed, coincidence events) are shown in Figure 8. The suppressed gamma-ray spectrum (black spectrum) from our previous modeling work (Farsoni et al., 2010) is shown in this figure as a reference.

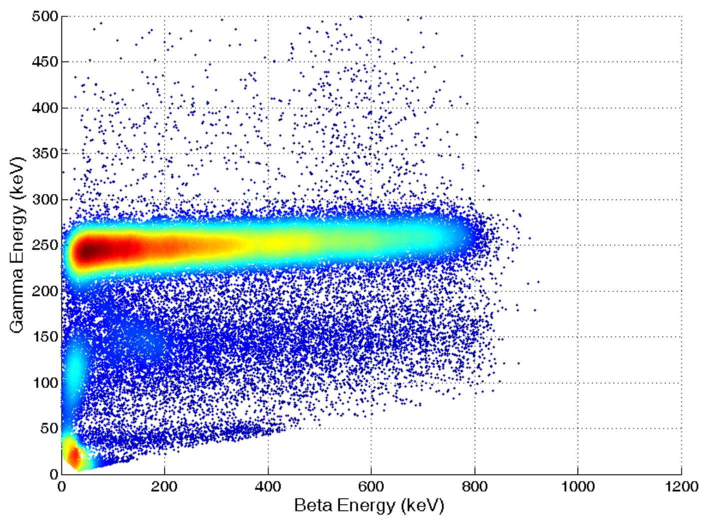

Figure 7. 2-D beta-gamma coincidence energy histograms from ^{135}Xe.

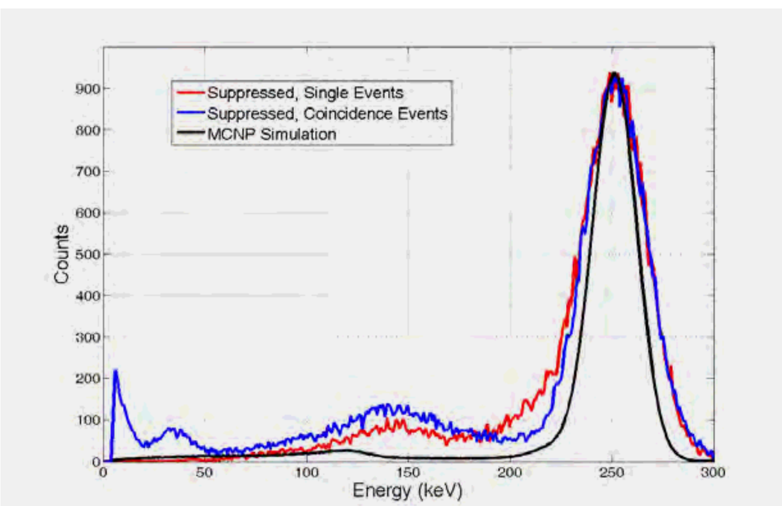

Figure 8. Gamma energy spectra in CsI(Tl) from ^{135}Xe. The red and blue spectra were updated from events in regions 2 (single events) and 3 (coincidence events), respectively. The black spectrum is a suppressed spectrum in CsI(Tl) and was obtained from our MCNP modeling (Farsoni et al., 2010).

Whereas the 250 keV photopeak in simulated spectrum shown in Figure 8 has a resolution of about 10%, the resolution for the same peak in both experimental spectrums was measured to be 13%. A small peak at about 40 keV in the suppressed-coincidence spectrum is believed to be due to some errors in pulse shape discrimination analysis and will be fixed in the future improvements. In our previous modeling work (Farsoni et al., 2010), no threshold was set for anti-coincidence process (suppression). This might be a reason why the shape is different around the Compton edge for the experimental and simulated spectra. In fact, when high-angle and low-energy scattered photons from CsI(Tl) are absorbed in the BGO, they produce very small flashes (BGO has a low light yield compared with CsI(Tl)) and may not be correctly detected and discriminated by the pulse shape discrimination process. This problem can be minimized by improving the overall light collection efficiency.

^{133}Xe measurements

Figure 9 shows the FCR-SCR scatter plot after ^{133}Xe was injected into the gas cell of the phoswich detector. For this experiment, the gas cell was fully sealed to avoid any leakage as explained before. The ^{133}Xe scatter plot shows much more events in region 1 (BC-400 signal events) and in region 3 (CsI-BC400 coincidence events) than in other regions. Here, region 4 (BGO single events) is clearly identified and isolated from other regions but has a wider distribution when it is compared with the ^{135}Xe scatter plot. This might be due to its lower gamma energy (30 keV and 80 keV) which eventually results in more uncertainty in pulse shape discrimination process.

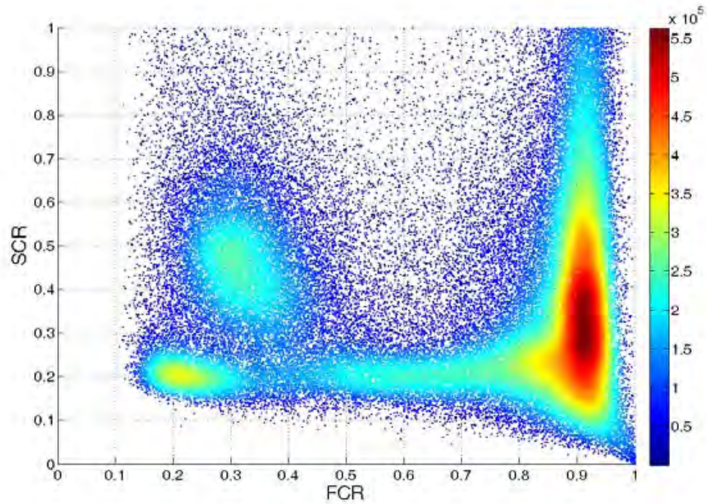

Figure 9. Scatter of Fast and Slow Component Ratios from ^{133}Xe.

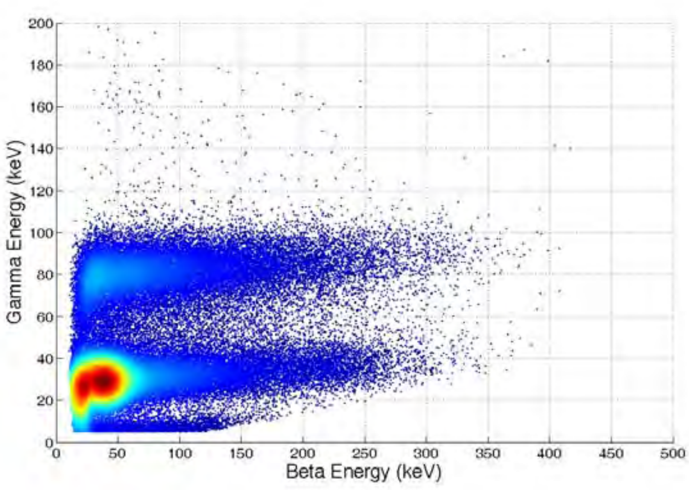

Figure 10. 2-D beta-gamma coincidence energy histograms from ^{133}Xe.

Results from Figure 9 was used to locate region 3 (beta-gamma coincidence events from ^{133}Xe) and collect the two-dimensional beta-gamma coincidence energy spectra depicted in Figure 10. Horizontal and vertical axes in this figure represent energy absorption in BC-400 and CsI(Tl), respectively. In this figure, 30 keV and 80 keV gamma lines are clearly populated and extend up to the maximum energy of beta particles from ^{133}Xe.

Figure 11 shows the beta-gated gamma-ray spectrum from ^{133}Xe. This spectrum was collected using events in region 3 (beta-gamma coincidence events) of the FCR-SCR scatter plot. The energy resolution for 30 keV and 80 keV peaks were measured to be 46% and 24%, respectively. In this spectrum, events below about 15 keV are from electrical noise.

Beta energy spectra gated with two regions of interest in the gamma energy spectrum of ^{133}Xe, 30 keV and 80 keV, are shown in Figure 12. The blue spectrum was processed from events in region 3 (beta-gamma coincidence events) when a beta event from the BC-400 is detected in coincidence with 30 keV x-ray from the CsI(Tl). The 30 keV-gated beta spectrum shows a peak at about 45 keV. This peak represents conversion electrons emitted in coincidence with 30 keV x-rays from ^{133}Xe. The red energy spectrum in Figure 12 was processed from events in region 3 of Figure 3 (beta-gamma coincidence events) when a beta event from the BC400 is in coincidence with an 80 keV gamma-ray from the CsI(Tl). The 80 keV-gated beta energy spectrum shows a beta continuum with no peak, as expected.

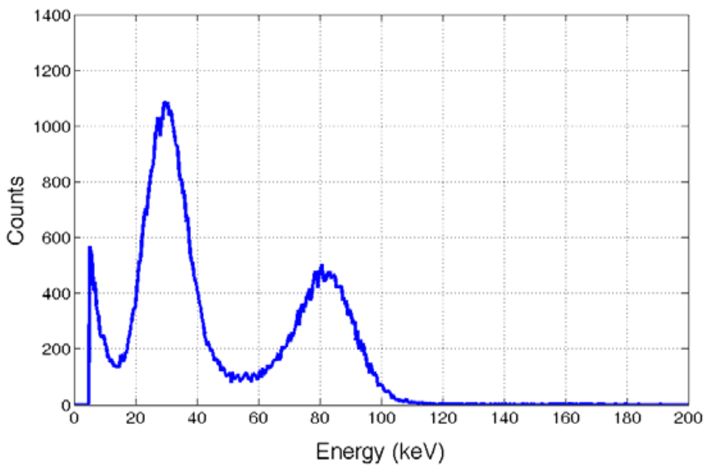

Figure 11. Gamma energy spectrum in CsI(Tl) from ^{133}Xe. The spectrum was collected from events in region 3 (beta-gamma coincidence) shown in Figure 3.

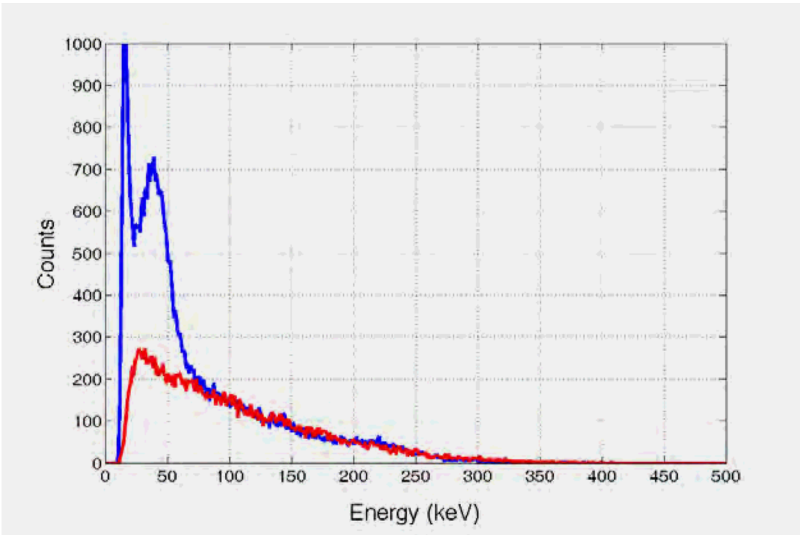

Figure 12. Beta energy histograms (BC-400) from ^{133}Xe in plastic scintillator gated with 30-keV X-rays (blue) and 80-keV gamma-rays (red).

CONCLUSION

We have developed and constructed a phoswich detector with Compton suppression capability for radioxenon measurements via beta-gamma coincidence technique. To have full flexibility in customizing the phoswich detector, we assembled the detector in our lab. A fully digital pulse processing algorithm was developed to discriminate different pulse shapes and radiation interaction events in the detector. The results from our recent measurements with lab sources and radioxenon gases generated in the Oregon State University TRIGA reactor were presented in this paper. Our preliminary measurements show that the Compton suppression mechanism reduces the Compton continuum from 662 keV photons by 50%-60% in the low-energy region of spectrum. Our beta-gamma coincidence measurements with ^{135}Xe and ^{133}Xe radioisotopes showed energy resolutions of 13%, 46% and 24% for 250 keV, 30keV and 80 keV gamma-ray peaks, respectively. Future work will be performed to enhance the overall performance of the phoswich detector, these will include (1) implementation of the current off-line digital pulse processing in the on-board FPGA device to achieve real-time xenon measurements, and (2) reassembling the phoswich detector with high-reflective wrapping materials around the scintillation assembly to gain better overall light collection efficiency.

REFERENCES

ANSI/IEEE Standard 325, Test Procedures for Germanium Gamma-ray Detectors, 1986.

Ely, J. H., C. E. Aalseth, J. C. Hayes, T. R. Heimbigner, J. I. McIntyre, H. S. Miley, M. E. Panisko, and M. Ripplinger (2003). Novel Beta-gamma coincidence measurements using phoswich detectors, in *Proceedings of the 25th Seismic Research Review – Nuclear Explosion Monitoring: Building the Knowledge Base*, LA-UR-03-6029, Vol. 2, pp. 533–541.

Farsoni, A. T., D. M. Hamby, C. S. Lee, and A. J. Elliott (2008). Preliminary experiments with a triple-layer phoswich detector for radioxenon detection, in *Proceedings of the 30th Monitoring Research Review: Ground-Based Nuclear Explosion Monitoring Technologies*, LA-UR-08-05261, Vol. 2, pp. 739–748.

Farsoni, A. T. and D. M. Hamby (2010). Design and modeling of a Compton-suppressed phoswich detector for radioxenon monitoring, in *Proceedings of the 2010 Monitoring Research Review: Ground-Based Nuclear Explosion Monitoring Technologies*, LA-UR-10-05578, Vol. 2, pp. 595–603.

Farsoni, A. T., and D. M. Hamby (2010). Characterizing a two-channel phoswich detector using radioxenon isotopes produced in the OSU TRIGA reactor, in *Proceedings of the 2010 Monitoring Research Review: Ground-Based Nuclear Explosion Monitoring Technologies*, LA-UR-10-05578, Vol. 2, pp. 585–594.

Hennig, W., H. Tan, W. K. Warburton, and J. I. McIntyre (2005). Digital pulse shape analysis with phoswich detectors to simplify coincidence measurements of radioactive xenon, in *Proceedings of the 27th Seismic Research Review: Ground-Based Nuclear Explosion Monitoring Technologies*, LA-UR-05-6407, Vol. 2, pp. 787–794.

McIntyre, J. I., K. H. Able, T. W. Bowyer, J. C. Hayes, T. R. Heimbigner, M. E. Panisko, P. L. Reeder, and R. C. Thompson (2001). Measurements of ambient radioxenon levels using the automated radioxenon sampler/analyzer (ARSA), *J. Radioanal. Nucl. Chem*. 248: 629–635.